

Prediction of the Band Structures of Bi₂Te₃-related Binary and Sb/Se-doped Ternary Thermoelectric Materials

Byungki Ryu,* Bong-Seo Kim, Ji Eun Lee, Sung-Jae Joo, Bok-Ki Min, HeeWoong Lee, and
Sudong Park

*Thermoelectric Conversion Research Center, Korea Electrotechnology Research Institute (KERI),
Changwon 51543, Republic of Korea*

Min-Wook Oh,
*Department of Advanced Materials Engineering, Hanbat National University, Daejeon 34158,
Republic of Korea*

Density functional calculations are performed to study the band structures of Bi₂Te₃-related binary (Bi₂Te₃, Sb₂Te₃, Bi₂Se₃, and Sb₂Se₃) and Sb/Se-doped ternary compounds [(Bi_{1-x}Sb_x)₂Te₃ and Bi₂(Te_{1-y}Se_y)₃]. The band gap was found to be increased by Sb doping and to be monotonically increased by Se doping. In ternary compounds, the change in the conduction band structure is more significant as compared to the change in the valence band structure. The band degeneracy of the valence band maximum is maintained at 6 in binaries and ternaries. However, when going from Bi₂Te₃ to Sb₂Te₃ (Bi₂Se₃), the degeneracy of the conduction band minimum is reduced from 6 to 2(1). Based on the results for the band structures, we suggest suitable stoichiometries of ternary compounds for high thermoelectric performance.

PACS numbers: 71.15.Mb, 71.20.-b, 71.20.Nr, 72.15.Jf

Keywords: Band structure, Thermoelectric, Bi-Sb-Te, Bi-Te-Se, DFT

Email: byungkiryu@keri.re.kr

Fax: +82-55-280-1590

I. INTRODUCTION

Tetradymite Bi_2Te_3 is the traditional thermoelectric (TE) material for direct energy conversion between heat and electricity [1, 2]. For the application of TE technology to waste heat recovery and solid state cooling, it is desired to have high performance *p*- and *n*-type TE materials. The TE energy conversion efficiency and performance are determined by the dimensionless figure of merit ZT defined as $(\alpha^2\sigma/\kappa)T$ [1, 2], where α , σ , κ , and T are the Seebeck coefficient, electrical conductivity, thermal conductivity, and absolute temperature, respectively. Therefore, high TE performance with high ZT can be achieved with a high power factor $\alpha^2\sigma$ (PF) and a small thermal conductivity κ . Many studies have been in the area of low-dimensionalization [3, 4], carrier energy filtering [5, 6] distortion of electronic density of states [7, 8], Fermi level tuning [9-12], band convergence [13, 14], and highly mismatched isoelectric doping [15] to improve the PF. Meanwhile, studies have been done on low total or lattice thermal conductivities in TE materials by using an intrinsically low κ [16, 17], point scattering by alloying [1, 18-20], formation of nano- to micro-structures [21-26], or Peierls distortion and charge density wave instabilities [27].

The electronic band structure is an important property of materials and determines the thermoelectric properties of the Seebeck coefficient α and the electrical conductivity σ . In a simple semi-classical electron transport model with parabolic band and the constant relaxation time approximation, the Seebeck coefficient is given by:

$$\alpha = (2/3e)(k_B\hbar)^2 (g\pi/3n)^{2/3} (m^*)T, \quad (1)$$

where g is the band valley degeneracy, n is the carrier concentration, and m^* is the effective mass of the single carrier pocket. Note that a high band degeneracy is necessary for high Seebeck coefficient. In addition, the band gap is an important factor and is strongly related to the bipolar effect. When the

temperature is increased, the thermal energy becomes comparable to the band gap, and the concentration of minority carrier increases. Thus, the Seebeck coefficient decreases and the thermal conductivity increases.

In a degenerate semiconductor, $|\alpha|$ decreases and σ increase when the carrier concentration and the Fermi level increase. Thus, an optimal carrier concentration for maximizing the PF exists. The optimal carrier concentration of Bi_2Te_3 is known to be about 10^{19} to 10^{20} cm^{-3} [10, 12], which corresponds to the heavily-doped system. The anti-site and vacancy defects are revealed to be the major acceptor and donor defects in Bi_2Te_3 -based materials [28-31].

In Bi_2Te_3 -based thermoelectric materials, the addition of Sb and Se elements is known to be an effective way to optimize the carrier concentration and to lower the thermal conductivity. Experimentally, the optimal stoichiometry is known to be $(\text{Bi}_{1-x}\text{Sb}_x)_2\text{Te}_3$ ($x=0.75$) for the *p*-type material and $\text{Bi}_2(\text{Te}_{1-y}\text{Se}_y)_3$ ($y\sim 0.15$) for the *n*-type material [1, 2, 30-33]. However, an understanding of why the ternary systems show better thermoelectric behavior than binary compounds is lacking. Although the band structures [34-46] and the thermoelectric transport properties [10, 11, 15, 37, 41-43, 45] have been studied extensively for binary Bi_2Te_3 , Sb_2Te_3 , Bi_2Se_3 , few theoretical studies of band structures and transport properties for Bi_2Te_3 -based *ternary* compounds have been done [12, 47, 48]. Moreover, minimal information on the band structure, i.e. the band degeneracies and band gaps, is available for ternary systems.

In this study, to understand the effect of Sb and Se alloying on the band structures in Bi_2Te_3 -based ternary compounds, we performed the density-functional-theory (DFT) electronic structure calculations [49, 50]. We considered various ternary compounds $[(\text{Bi}_{1-x}\text{Sb})_2\text{Te}_3$ and $\text{Bi}_2(\text{Te}_{1-y}\text{Se}_y)_3]$. The band gaps and the band degeneracies of the band edges were investigated for ternary systems, within virtual crystal approximation (VCA) [51]. Based on the results, we suggest an optimal stoichiometry for Bi_2Te_3 -based ternary TE compounds.

II. CALCULATION METHOD

First-principles density functional calculations were performed to study the electronic structure of the Bi_2Te_3 based thermoelectric materials. The generalized-gradient-approximation parameterized by Perdue, Burke, and Ernzerhof (PBE) [52] and the projector augmented wave (PAW) pseudopotentials [53] were used, as implemented in Vienna-Ab-initio-Simulation-Package (VASP) code [54, 55]. For Bi, Sb, Te, and Se, the outermost s and p electrons are considered as valence electrons. The energy cutoff is 250 eV. The experimental lattice parameter and theoretically optimized internal coordinates are used for binary Bi_2Te_3 , Sb_2Te_3 , and Bi_2Se_3 . In the case of Sb_2Se_3 , the stable structure is the orthorhombic structure. For the comparison with layered Bi_2Te_3 , the tetradymite Bi_2Te_3 atomic structure was used for Sb_2Se_3 . The lattice parameters were obtained by using the following equations:

$$a[\text{Sb}_2\text{Se}_3] = a[\text{Sb}_2\text{Te}_3] + a[\text{Bi}_2\text{Se}_3] - a[\text{Bi}_2\text{Te}_3], \quad (2)$$

and the internal parameter was also relaxed for Sb_2Se_3 . For ternary alloys of $(\text{Bi}_{1-x}\text{Sb})_2\text{Te}_3$ (**BST**) and $\text{Bi}_2(\text{Te}_{1-y}\text{Se}_y)_3$ (**BTSe**), the lattice parameters and the internal coordinates were interpolated from those for binary compounds. To reduce the heavy computational cost of alloying supercell, we used the primitive unit cell with the VCA. To validate the VCA results, we also tested the $(2 \times 2 \times 1)$ 20-atom alloy supercell for the band-gap calculations and found that the tendency of the band-gap change were maintained. The Monkhorst-Pack k -point mesh [56] of gamma-centered $36 \times 36 \times 36$ per primitive cell was used. The spin orbit interaction (SOI) was included when calculating the band structures.

III. RESULTS AND DISCUSSION

The atomic structure of tetradymite- Bi_2Te_3 is a layered structure and is categorized in the space group $R\bar{3}m$ (No. 166). As shown in the **Figure 1**, two Bi and three Te atoms are stacked with an ABCAB stacking sequence and they form a quintuple layer (QL). The rhombohedral primitive cell contains two inequivalent Te atoms: two Te(1) atoms at the QL surfaces and one Te(2) atom at the

center of the QL. The Bi atoms are surrounded by three Te(1) and three Te(2) atoms, forming the local structure of octahedral Bi-Te₆. Three QLs are contained in a conventional hexagonal unit cell. **Table 1** shows the details of the atomic structures of Bi₂Te₃, Sb₂Te₃, Bi₂Se₃, and Sb₂Se₃ binary compounds.

The electronic structure of the Bi₂Te₃, Sb₂Te₃, Bi₂Se₃, and Sb₂Se₃ binary materials were calculated. Without the spin orbit interaction (SOI), all system had a direct band gap at the Γ k -point with band degeneracy (g) of 1. As a result, the SOI interaction at Γ was the strongest compared to other k -points. The band structures of Bi₂Te₃, Sb₂Te₃, Bi₂Se₃ and Sb₂Se₃ binary compounds are shown in **Table 1 and Figure 2**. First, we predicted the band gap. For the PBE calculations without SOI, the E_g^{PBE} was the largest for Bi₂Te₃. With SOI, the PBE gap (E_g^{SOI}) decreased to 0.104 eV for Bi₂Te₃ and increased to 0.111 eV for Sb₂Te₃. For Bi₂Se₃, the band gap were nearly maintained. Our result is consistent with those in other DFT reports [39, 44], but still underestimated compared to the experimental values [36, 44, 57, 58] The band gap of Sb₂Se₃ was found to be 0.201 eV. With the inclusion of SOI, the k -points of the valence band maximum (VBM) and conduction band minimum (CBM) (k_{VBM} and k_{CBM}) changed and were not on the high symmetry points and lines. As a result, band degeneracies of VBM and CBM (g_{VBM} and g_{CBM}) changed. To predict the k_{VBM} and k_{CBM} , here we used the 46656 k -points (gamma centered 36×36×36) for the 5-atom binary system. Note that, for all binary compounds, the g_{VBM} is always 6, similar to other results [1, 36, 39-41]. However the g_{CBM} is not identical for binaries. For Bi₂Te₃ and Sb₂Se₃, the VBM and CBM are at the same k -points, showing a direct band gap. In contrary, Sb₂Te₃ and Sb₂Se₃ have the indirect band gap. For Sb₂Te₃, the k of CBM is located on the middle of the Γ Z line in Brillouin zone and the band degeneracy is only 2. In the case of Bi₂Se₃, the CBM is at Γ . We'd like to mention that the g_{CBM} can be sensitive to the choice of pseudopotentials or exchange-correlation energies and can vary from 6 to 2(1) due to the small energy difference between local minima [35, 40]. Note that our density functional calculation result of $g_{\text{CBM}} = 6$ for Bi₂Te₃ is consistent to that from recent quasiparticle GW approximation calculations [40].

The electronic structures of (Bi_{1-x}Sb_x)₂Te₃ ($x = 0$ to 1) and Bi₂(Te_{1-y}Se_y)₃ ($y = 0$ to 1) alloys were

investigated. All lattice parameters and internal parameters were linearly interpolated by using the values for binaries. We adopted the VCA when calculating the electronic structures. The disordered ternary systems were considered as ordered binary systems with interpolated atomic potentials, ignoring any possible short range ordering. [Figure 3](#) shows the E_g^{SOI} for $(\text{Bi}_{1-x}\text{Sb})_2\text{Te}_3$ and $\text{Bi}_2(\text{Te}_{1-y}\text{Se}_y)_3$ ternary alloy compounds for gamma-centered k -point meshes of $6\times6\times6$, $12\times12\times12$, $24\times24\times24$, and $36\times36\times36$. Note that the very fine k -point mesh is mandatory to ensure the convergence of the band gap for Bi_2Te_3 -based ternary compounds as well as for binary compounds. The band-energy convergence with respect to the k -point mesh were calculated to be less than 1 meV. We found that the band gap of E_g^{SOI} was increased by alloying with Sb and Se elements. The E_g^{SOI} of Sb_2Te_3 was larger than that of Bi_2Te_3 by 0.012 eV. The band gap of **BST** increased with increasing x and became maximum at $x = 30\text{--}70\%$. On the other hand, the band gap of **BTSe** monotonically increased from 0.105 to 0.260 eV when going from Bi_2Te_3 to Bi_2Se_3 .

By comparing the VCA band gap with the supercell band gaps, we verified the reliability of the band gap of the primitive cell with the VCA. For BST and BTSe, we used the $(2\times2\times1)$ 20-atom supercell for BST and BTS that contained 8 Bi/Sb atoms and 12 Te/Se atoms. We considered 12 different atomic configurations for the $\text{Bi}_{8-n}\text{Sb}_n\text{Te}_{12}$ supercells (n is an integer from 0 to 8) and 25 configurations for the $\text{Bi}_8\text{Te}_{12-m}\text{Se}_m$ (m is an integer from 0 to 12) supercells. In the modelled structures, the lattice parameters and the internal parameters were interpolated from those for binary structures. The values of E_g^{SOI} from the VCA and the supercell approaches are compared in [Figure 4](#). The supercell band gap was calculated to be smaller than the VCA band gap. We think that the disorder-induced charge-density-localization in a finite supercell might be responsible for the band-gap variation in the supercell calculations, as compared to the VCA results. For that reason, we calculated and used the fitting curves for the BST and the BTSe band gaps. For **BST**, the fitted band-gap curve, represented by dashed line, is nearly the same as that for supercell approach. However, for **BTSe**, the tendency of the fitted band gap change is still valid.

Next, the positions of the VBM and the CBM were examined for ternary compounds. **Figure 5** represents the positions of the VBM and the CBM, k_{VBM} and k_{CBM} , for the **BST** and the **BTSe** alloys. We found that the change in k_{CBM} was significant when alloying while the change in k_{VBM} was relatively small due to the valence band shapes being similar among the binary compounds. For small x and y , the **BST** and the **BTSe** band edges are located near the k_{VBM} and the k_{CBM} of Bi_2Te_3 . However, as x and y were increased, the band edges moved toward the k_{VBM} and the k_{CBM} of Sb_2Te_3 and Bi_2Se_3 , respectively. For Bi_2Te_3 , the band degeneracy of the VBM and the CBM was 6. We found that the band degeneracy $g_{\text{VBM}} = 6$ is robust against the Bi_2Te_3 alloying with Sb_2Te_3 and Bi_2Se_3 . To the contrary, g_{CBM} changed when alloying. For **BST**, the g_{CBM} was 6 for $x = 0.0 - 0.2$ and the g_{CBM} was 2 for $x = 0.3 - 1.0$. For **BTS**, the g_{CBM} was 6 for $y = 0.0 - 0.3$, the g_{CBM} was 2 for $y = 0.4 - 0.6$, and the $g_{\text{CBM}} = 1$ when $y = 0.7 - 1.0$.

For high thermoelectric performance, a large power factor and a small thermal conductivity are needed. The power factor is maximized with optimal band structures with high band degeneracy, relatively large band gap, and proper position of the Fermi level. Based on calculated results, band gaps and band degeneracies of Bi_2Te_3 -based ternary alloys, we suggest a suitable stoichiometry for high thermoelectric performance. For *p*-type **BST**, the band degeneracy is maintained for all stoichiometry. If our VCA band gap is correct, $(\text{Bi}_{1-x}\text{Sb})_2\text{Te}_3$ with $x = 0.3 - 0.7$ seems to be good, which might be responsible for the smaller bipolar effect on Seebeck coefficient and the thermal conductivity. However, if the supercell band gap is correct, there should be a band gap reduction and the increase of bipolar effect in Seebeck coefficient and the electrical thermal conductivity. In this case, the role of Sb-doping/alloying in Bi_2Te_3 is to generate the *p*-type carriers by the formation of anti-site defects and a reduction in the lattice thermal conductivity caused by point disorder. For *n*-type **BTSe**, $\text{Bi}_2(\text{Te}_{1-y}\text{Se}_y)_3$ with $y = 0.3$ is the best due to its having the largest band gap among the high-CBM-degeneracy alloys ($g_{\text{CBM}} = 6$). We find that our suggested stoichiometries for **BST** and **BTSe** ($x = 0.3 - 0.7$, $y = 0.3$) are consistent with the stoichiometries used in experiments ($x = 0.75$, $y = \sim 0.15$) [1, 2, 30, 33]. Note that

here we only consider the band gaps and the band degeneracy and do not consider the reduction in the lattice thermal conductivity in disordered alloy ternary compounds. If we consider the reduction in the lattice thermal conductivity caused by point disorder in ternary compounds, we may conclude that the thermoelectric property of ternary compounds is superior to that of binary compounds.

IV. CONCLUSION

In conclusion, we investigated the electronic structures of Bi_2Te_3 -based ternary alloys within density functional theory and the virtual crystal approximation. The band degeneracy, the band gap, and the positions of the band edges of $(\text{Bi}_{1-x}\text{Sb})_2\text{Te}_3$ and $\text{Bi}_2(\text{Te}_{1-y}\text{Se}_y)_3$ were systemically examined. The band gap was found to be increased by Sb doping and to be monotonically increased by Se doping. For p -type **BST**, the valence band degeneracy were maintained. However, for n -type **BTSe**, the conduction band degeneracy was very sensitive to the alloy stoichiometry. Based on the results, we suggest a suitable stoichiometry of Bi_2Te_3 -based ternary alloys for better thermoelectric performance.

ACKNOWLEDGMENTS

This research was supported by Korea Electrotechnology Research Institute (KERI) Primary research program through the National Research Council of Science & Technology (NST) funded by the Ministry of Science, ICT and Future Planning (MSIP) [No. 15-12-N0101-24, *Development of design tools of thermoelectric and energy materials*] and by the IT R&D program of Korea Evaluation Institute of Industrial Technology (KEIT) funded by Ministry of Trade, Industry and Energy (MOTIE) [No. 10048035, *Development of Bi-Te based Thermoelectric Energy Conversion Materials by Controlling Multi-level Nanostructure in Pilot Scale*].

REREFENCES

- [1] H. J. Goldsmid, *Introduction to Thermoelectricity* (Springer, Berlin, Heidelberg, 2010).
- [2] D. M. Rowe, *Thermoelectrics Handbook* (CRC Press, Boca Raton, 2006).
- [3] L. D. Hicks and M. S. Dresselhaus, Phys. Rev. B **47**, 12727 (1993).
- [4] M. S. Dresselhaus, G. Chen, M. Y. Tang, R. Yang, H. Lee, D. Wang, Z. Ren, J.-P. Fleurial, and P. Gogna, Adv. Mater. **19**, 1043 (2007).
- [5] J. M. O. Zide, D. Vashaee, Z. X. Bian, G. Zeng, J. E. Bowers, A. Shakouri, and A. C. Gossard, Phys. Rev. B **74**, 205335 (2006).
- [6] S. V. Faleev and F. Léonard, Phys. Rev. B **77**, 214304 (2008).
- [7] G. D. Mahan and J. O. Sofo, Proc. Natl. Acad. Sci. U.S.A. **93**, 7436 (1996).
- [8] J. P. Heremans, V. Jovovic, E. S. Toberer, E. A. Saramat, K. Kurosaki, A. Charoenphakdee, S. Yamanaka, and G. J. Snyder, Science **321**, 554 (2008).
- [9] G. J. Snyder and E. S. Toberer, Nature Mater. **7**, 105 (2008).
- [10] T. J. Scheidemantel, C. Ambrosch-Draxl, T. Thonhauser, J. V. Badding, and J. O. Sofo, Phys. Rev. B **68**, 125210 (2003).
- [11] M. W. Oh, D. M. Wee, S. D. Park, B. S. Kim, and H. W. Lee, Phys. Rev. B **77**, 165119 (2008).
- [12] S. Feng, S. Li, X. Li, and Hengzhi Fu, Comp. Mater. Sci. **95**, 563 (2014).
- [13] Y. Pei, X. Shi, A. LaLonde, H. Wang, L. Chen, and G. J. Snyder, Nature (London) **473**, 66 (2011).
- [14] W. Liu, X. Tan, K. Yin, H. Liu, X. Tang, J. Shi, Q. Zhang, and C. Uher, Phys. Rev. Lett. **108**, 166601 (2012).
- [15] J.-H. Lee, J. Wu, and J. C. Grossman, Phys. Rev. Lett. **104**, 016602 (2010).
- [16] L.-D. Zhao, S.-H. Lo, Y. Zhang, H. Sun, G. Tan, C. Uher, C. Wolverton, V. P. Dravid, and G. Kanatzidis, Nature (London) **508**, 373 (2014).

- [17] D. T. Morelli, V. Jovovic, and J. P. Heremans, Phys. Rev. Lett. **101**, 035901 (2008).
- [18] B. Abeles, Phys. Rev. **131**, 1906 (1963).
- [19] M. C. Steele and F. D. Rosi, J. Appl. Phys. **29**, 1517 (1958).
- [20] J. Garg, N. Bonini, B. Kozinsky, and N. Marzari, Phys. Rev. Lett. **106**, 045901 (2011).
- [21] K. F. Hsu, S. Loo, F. Guo, W. Chen, J. S. Dyck, C. Uher, T. Hogan, E. K. Polychroniadis, and M. G. Kanatzidis, Science **303**, 818 (2004).
- [22] W. Kim, J. Zide, A. Gossard, D. Klenov, S. Stemmer, A. Shakouri, and A. Majumdar, Phys. Rev. Lett. **96**, 045901 (2006).
- [23] B. Poudel, Q. Hao, Y. Ma, Y. Lan, A. Minnich, B. Yu, X. Yan, D. Wang, A. Muto, D. Vashaee, X. Chen, J. Liu, M. S. Dresselhaus, G. Chen, and Z. Ren, Science **320**, 634 (2008).
- [24] K. Biswas, J. He, I. D. Blum, C.-I. Wu, T. P. Hogan, D. N. Seidman, V. P. Dravid, and M. G. Kanatzidis, Nature (London) **489**, 414 (2012).
- [25] R. J. Korkosz, T. C. Chasapis, S.-H. Lo, J. W. Doak, Y. J. Kim, C.-I. Wu, E. Hatzikraniotis, T. P. Hogan, D. N. Seidman, c. Wolverton, V. P. Dravid, and M. G. Kanatzidis, J. Am. Chem. Soc. **136**, 3225 (2014).
- [26] H. Wang, J.-H. Bahk, C. Kang, J. Hwang, K. Kim, J. Kim, P. Burke, J. E. Bowers, A. C. Gossard, A. Shakouri, and W. Kim, Proc. Natl. Acad. Sci. U.S.A. **111**, 10949 (2014).
- [27] J.-S. Rhyee, K. H. Lee, S. M. Lee, E. Cho, S. I. Kim, E. Lee, Y. S. Kwon, J. H. Shim, and G. Kotliar, Nature (London) **459**, 965 (2009).
- [28] S. Cho, Y. Kim, A. DiVenere, G. K. Wong, J. B. Ketterson, and J. R. Meyer, Appl. Phys. Lett. **75**, 1401 (1999).
- [29] D. West, Y. Y. Sun, H. Wang, J. Bang, and S. B. Zhang, Phys. Rev. B **86**, 121201(R) (2012).
- [30] J. H. Son, M. W. Oh, B. S. Kim, S. D. Park, B. K. Min, M. H. Kim, and H. W. Lee, J. Alloys Comp. **566**, 168 (2013).
- [31] M. W. Oh, J. H. Son, B. S. Kim, S. D. Park, B. K. Min, and H. W. Lee, J. Appl. Phys. **115**,

133706 (2014).

[32] G.-E. Lee, I.-H. Kim, S.-M. Choi, Y. S. Lim, W.-S. Seo, J.-S. Park, and S.-H. Yang, J. Korean Phys. Soc. **65**, 2066 (2014).

[33] G.-E. Lee, I.-H. Kim, S.-M. Choi, Y. S. Lim, W.-S. Seo, J.-S. Park, and S.-H. Yang, J. Korean Phys. Soc. **65**, 1908 (2014).

[34] P. Larson, S. D. Mahanti, M. G. Kanatzidis, Phys. Rev. B **61**, 8162 (2000).

[35] S. J. Youn and A. J. Freeman, Phys. Rev. B **63**, 085112 (2001).

[36] M. Kim, A. J. Freeman, C. B. Geller, Phys. Rev. B **72**, 035205 (2005).

[37] S. Lee and P. von Allmen, Appl. Phys. Lett. **88**, 022107 (2006).

[38] P. Larson, Phys. Rev. B **74**, 205113 (2006).

[39] G. Wang and T. Cagin, Phys. Rev. B **76**, 075201 (2007).

[40] E. Kioupakis, M. L. Tiago, and S. G. Louie, Phys. Rev. B **82**, 245203 (2010).

[41] B. Y. Yavorsky, N. F. Hinsche, I. Mertig, and P. Zahn, Phys. Rev. B **84**, 165208 (2011).

[42] N. F. Hinsche, B. Y. Yavorsky, I. Mertig, and P. Zahn, Phys. Rev. B **84**, 165214 (2011).

[43] D. Parker, and D. J. Singh, Phys. Rev. X **1**, 021005 (2011).

[44] O. V. Yazyev, E. Kioupakis, J. E. Moore, and S. G. Louie, Phys. Rev. B **85**, 161101(R) (2012).

[45] X. Luo, M. B. Sullivan, and S. Y. Quek, Phys. Rev. B **86**, 184111 (2012).

[46] I. A. Nechaev and E. V. Chulkov, Phys. Rev. B **88**, 165135 (2013).

[47] H. Y. Lv, H. J. Liu, L. Pan, Y. W. Wen, X. J. Tan, J. Shi, and X. F. Tang, Appl. Phys. Lett. **96**, 142101 (2010).

[48] M. S. Park, J.-W. Song, J. E. Medvedeva, M. Kim, I. G. Kim, and A. J. Freeman, Phys. Rev. B **81**, 155211 (2010).

[49] P. Hohenberg, and W. Kohn, Phys. Rev. **136**, B864 (1964).

[50] W. Kohn and L. J. Sham, Phys. Rev. **140**, A1133 (1965).

[51] L. Bellaiche and D. Vanderbilt, Phys. Rev. B **61**, 7877 (2000).

- [52] J. P. Perdew, K. Burke, and M. Ernzerhof, Phys. Rev. Lett. **77**, 3865 (1996).
- [53] P. E. Blöchl, Phys. Rev. B **50**, 1793 (1994).
- [54] G. Kresse and J. Furthmüller, Phys. Rev. B **54**, 11169 (1996).
- [55] G. Kresse and J. Joubert, Phys. Rev. **59**, 1758 (1999).
- [56] H. J. Monkhorst and J. D. Pack, Phys. Rev. B **13**, 5188 (1976).
- [57] R. Sehr and L. R. Testardi, J. Phys. Chem. Sol. **23**, 1219 (1962).
- [58] H. Zhang, C.-X. Liu, X.-L. Qi, X. Dai, Z. Fang, and S.-C. Zhang, Nature Phys. **5**, 438 (2009).

Table 1. Atomic and electronic structure table of binary Bi_2Te_3 , Sb_2Te_3 , Bi_2Se_3 , and Sb_2Se_3 compounds. a and c are the lattice constants of the conventional hexagonal unit cell, where $\|\mathbf{a}_{\text{RHL}}\|$ is the length of the rhombohedral lattice vector and $\cos \alpha$ is the directional cosine between the rhombohedral lattice vectors. u and v are internal coordinates for Bi and Te(1). E_g^{SOI} and E_g^{PBE} are the PBE band gap with and without spin-orbit-interaction (SOI). The band degeneracies (g) of the VBM and the CBM are denoted by g_{VBM} and g_{CBM} . The type of band gap (type of E_g) is classified as the direct and indirect gaps. The \mathbf{k} -points of the VBM and the CBM are denoted as \mathbf{k}_{VBM} and \mathbf{k}_{CBM} . All \mathbf{k} vectors are represented by using the basis of the reciprocal lattices.

	Bi_2Te_3	Sb_2Te_3	Bi_2Se_3	Sb_2Se_3
a (Å)	4.383	4.250	4.138	4.004*
c (Å)	30.487	30.400	28.640	28.553*
$\ \mathbf{a}_{\text{RHL}}\ $ (Å)	10.473	10.426	9.841	9.794
$\cos \alpha$	0.912	0.917	0.912	0.916
u	0.400	0.399	0.401	0.399
v	0.210	0.211	0.211	0.212
E_g^{PBE} (eV)	0.271	0.027	0.185	0.174
E_g^{SOI} (eV)	0.105	0.133	0.260	0.201
g_{VBM}	6	6	6	6
g_{CBM}	6	2	1	6
Type of E_g	Direct	Indirect	Indirect	Direct
\mathbf{k}_{VBM}	(.417, .417, .333)	(.389, .389, .333)	(.361, .361, .278)	(.028, .028, .028)
\mathbf{k}_{CBM}	(.417, .417, .333)	(.194, .194, .194)	(0, 0, 0)	(.028, .028, .028)

Figure Captions.

Fig. 1. Ball and stick model of the atomic structure of Bi_2Te_3 . Bi/Sb atoms are denoted by large balls, and Te/Se atoms are denoted by smaller ones. The Bi/Sb atoms are surrounded by six Te/Se atoms: three Te/Se(1) at QL surfaces and three Te/Se(2) at the center of the QL.

Fig. 2. Band structures are drawn for (a) Bi_2Te_3 , (b) Sb_2Te_3 , (c) Bi_2Se_3 , and (4) Sb_2Se_3 binary compounds in a tetradymite rhombohedral structure. The E_{VBM} is set to zero. The dashed vertical lines indicate E_{CBM} and E_{VBM} . The \mathbf{k} -point **a** corresponds to (0.43, 0.43, 0.64) on the basis of the reciprocal lattices.

Fig. 3. The $E_{\text{g}}^{\text{SOI}}$ for (a) $(\text{Bi}_{1-x}\text{Sb})_2\text{Te}_3$ and (b) $\text{Bi}_2(\text{Te}_{1-y}\text{Se}_y)_3$ ternary alloy compounds for gamma centered k -point meshes of $6 \times 6 \times 6$, $12 \times 12 \times 12$, $24 \times 24 \times 24$, and $36 \times 36 \times 36$. The dashed horizontal lines represent the band gaps of the binary compounds.

Fig. 4. The $E_{\text{g}}^{\text{SOI}}$ for (a) $(\text{Bi}_{1-x}\text{Sb})_2\text{Te}_3$ and (b) $\text{Bi}_2(\text{Te}_{1-y}\text{Se}_y)_3$ obtained by using the VCA approach (filled circles) and the supercell approach (open circles). The solid and the dashed lines are lines fitted to the band gaps obtained by using the VCA and the supercell approach, respectively.

Fig. 5. The positions of band edges are mapped for (a) $(\text{Bi}_{1-x}\text{Sb})_2\text{Te}_3$ and (b) $\text{Bi}_2(\text{Te}_{1-y}\text{Se}_y)_3$. \mathbf{b}_1 , \mathbf{b}_2 , and \mathbf{b}_3 are the reciprocal vectors for the given rhombohedral system. \mathbf{k}_{VBM} and \mathbf{k}_{CBM} are represented by filled circles and X marks, respectively. The numbers in the figures are the compositional ratios of the BST and the BTS alloys. For BST and BTS, the movement of \mathbf{k}_{CBM} is significant as compared to that of \mathbf{k}_{VBM} .

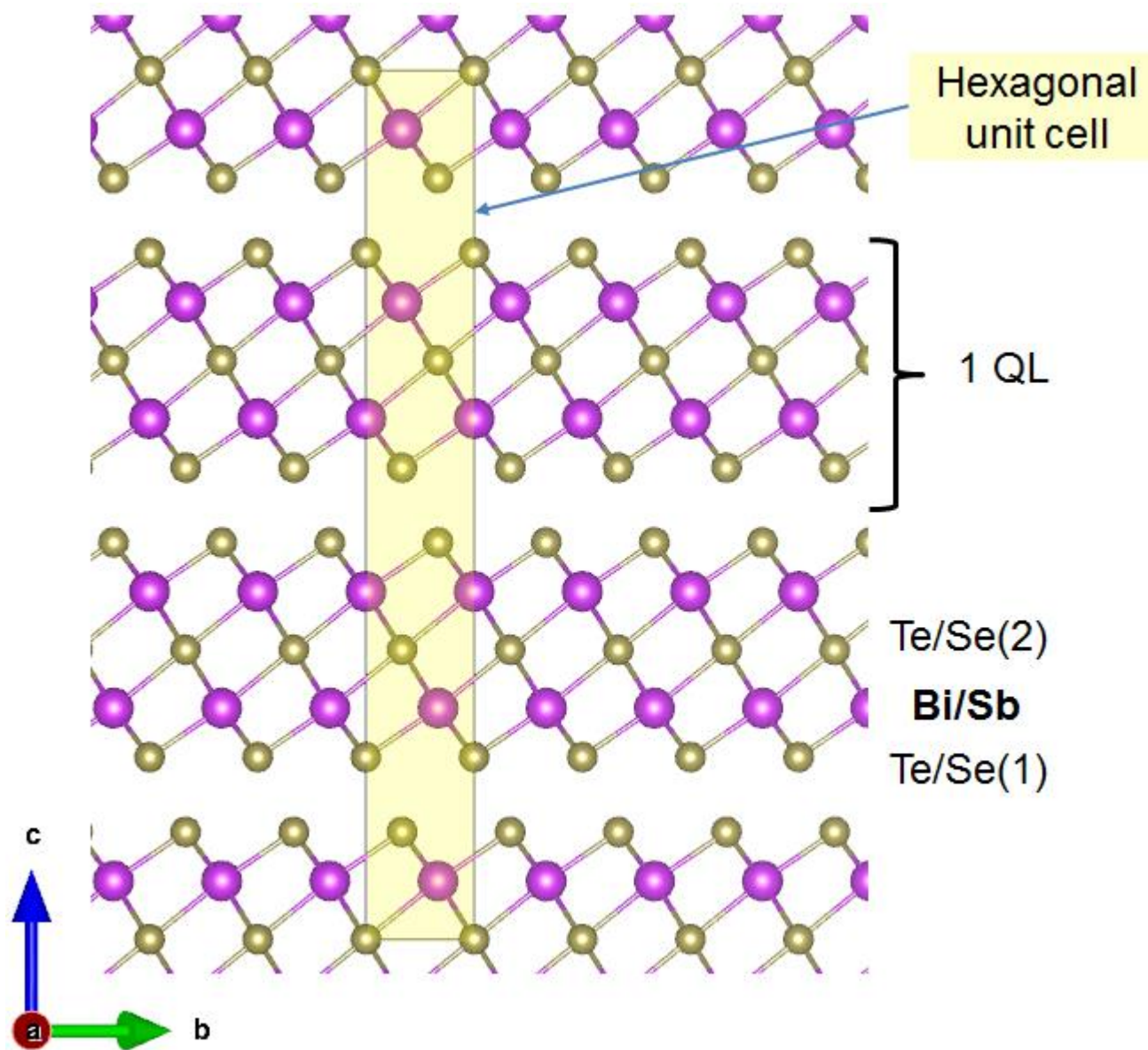


Figure 1

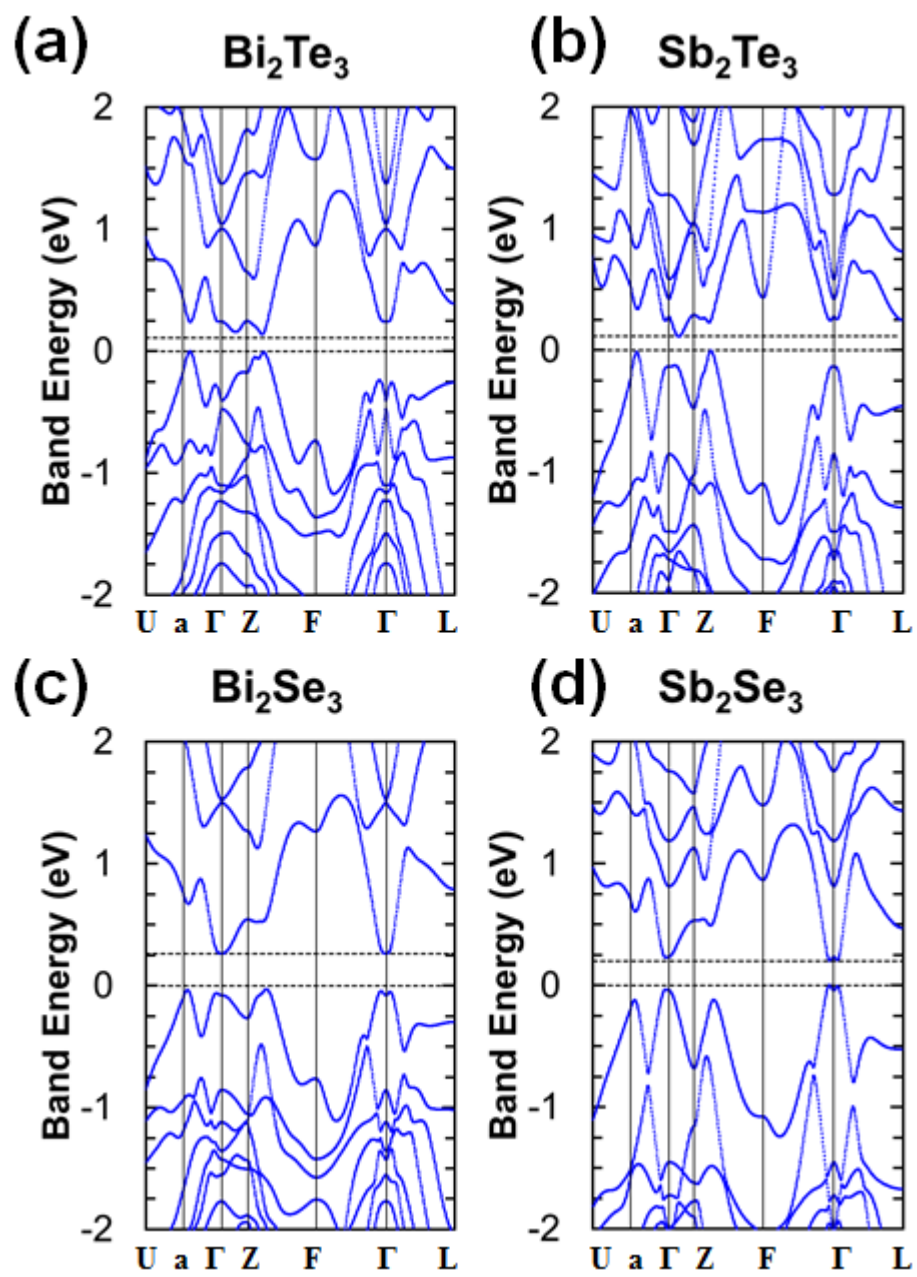


Figure 2

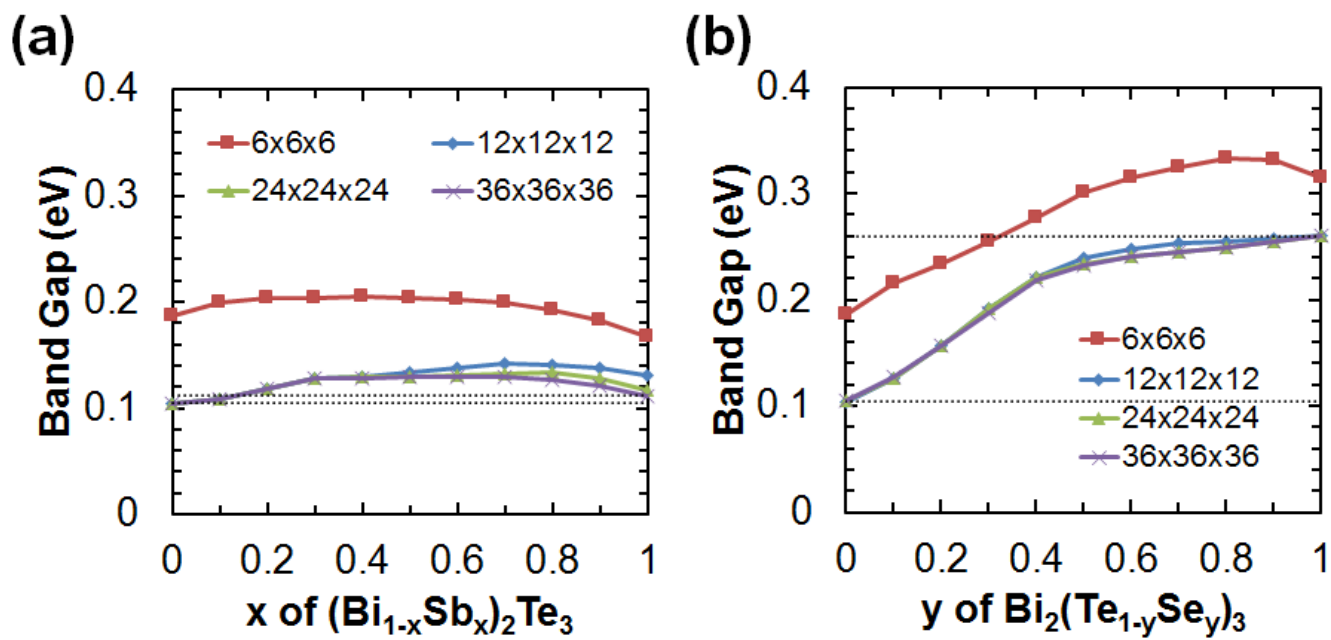


Figure 3

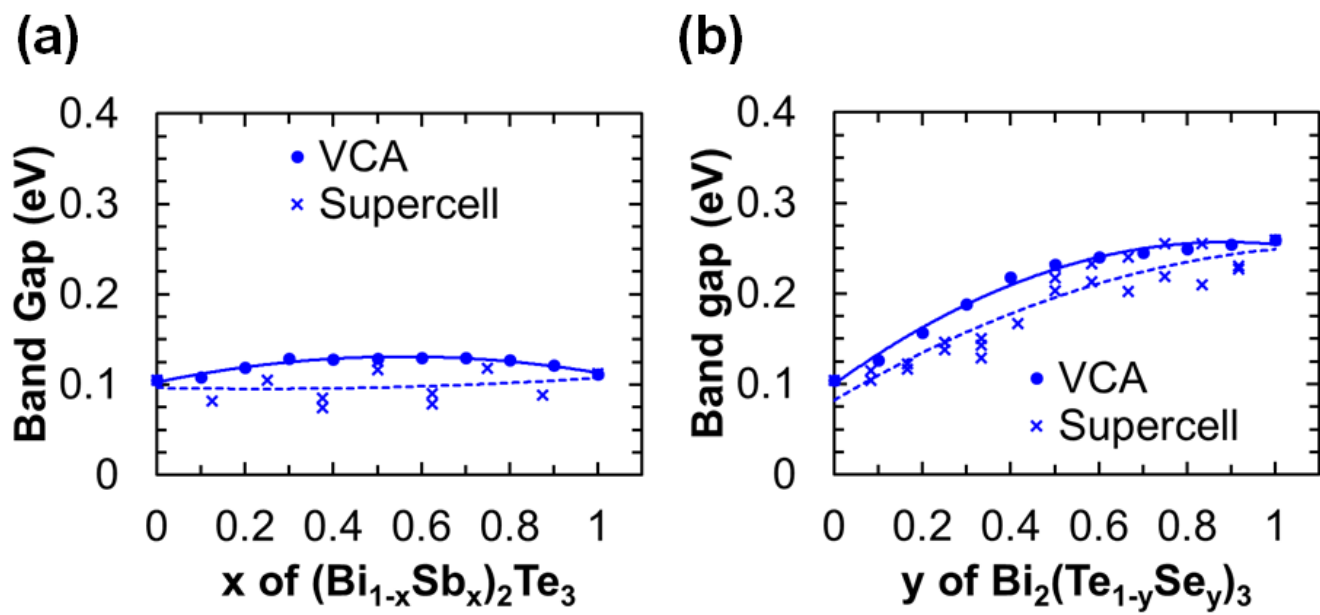


Figure 4

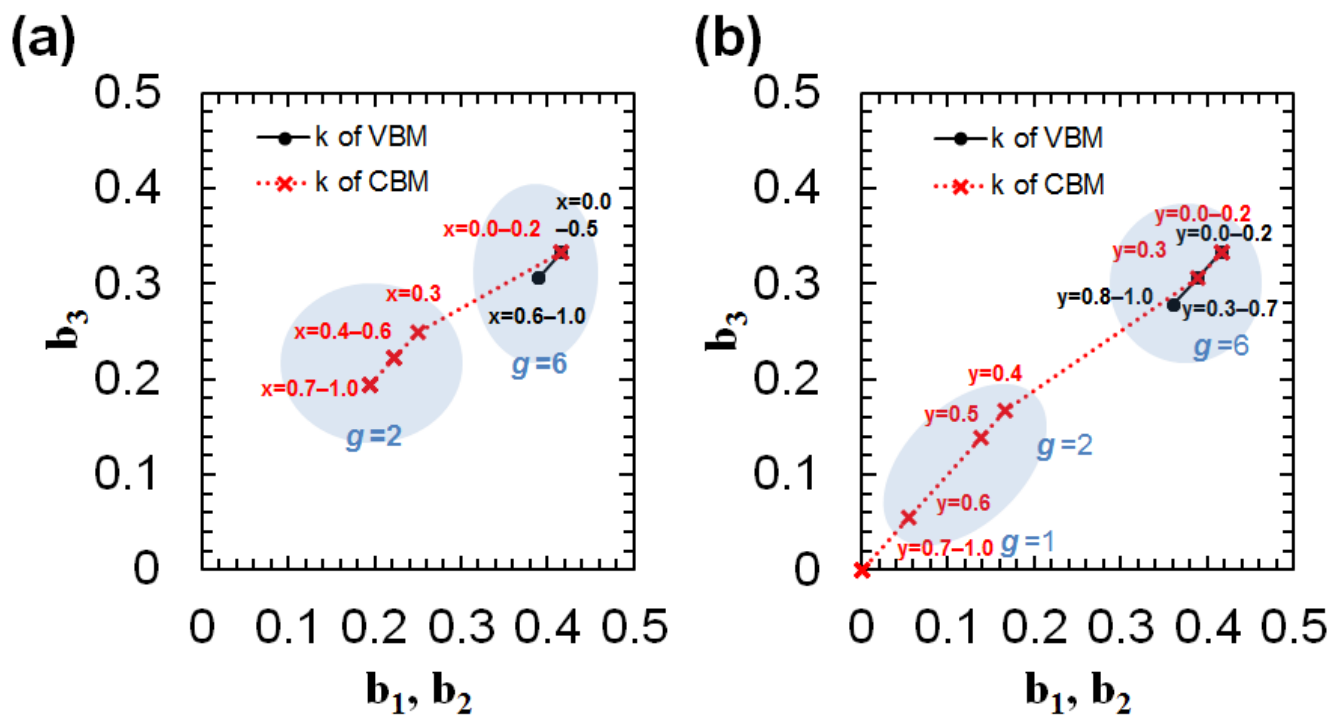


Figure 5